Korean J. Chem. Eng., 32(7), 1405-1413 (2015)
DOI: 10.1007/s11814-014-0336-4

pISSN: 0256-1115
eISSN: 1975-7220

Adsorption equilibrium, kinetics and mechanism studies of mercury on coal-fired fly ash

Qiang Zhou, Yufeng Duan†, Chun Zhu, Jun Zhang, Min She, Hongqi Wei, and Yaguang Hong

Key Laboratory of Energy Thermal Conversion and Control of Ministry of Education, School of Energy and Environment, Southeast University, Nanjing 210096, China
(*Received 21 August 2014 • accepted 13 November 2014*)

Abstract−Fly ash samples were collected from the electrostatic precipitator (ESP) of a 600 MW pulverized coal boiler firing Zhungeer bituminous coal in China to evaluate and explore its mercury adsorption capacity and mechanism. Samples characterization was conducted to feature their morphologies correlated to mercury content, and experimental studies on mercury adsorption in a fixed-bed apparatus were carried out to further verify its mercury adsorption availability. Based on the experimental data, adsorption isotherm was modeled with Langmuir, Freundlich, and Temkin equations. Adsorption kinetic analysis was also performed. The results show that mercury content of fly ash samples is associated with particle size, unburned carbon content and functional groups of Al-O/Si-O or Si-O-Si/Si-O-Al tetrahedron on fly ash. Increase of initial mercury concentration is beneficial to promote mercury adsorption due to the enhancement of mercury diffusion force onto the fly ash surface, mercury intraparticle diffusion rate and initial mercury adsorption rate. Fly ash with medium size displays better mercury adsorption capacity. Smaller particle size results in higher specific surface area, but brings about low specific surface area utilization rate for mercury adsorption. Freundlich isotherm equation presents better fitting result, indicating that fly ash surface is non-uniform. Mercury adsorption on fly ash at 120 °C is mainly physisorption enhanced by chemisorption with ΔG at −36.73 kJ/mol. The pseudo-first-order kinetic model can describe the adsorption process more accurately and predict mercury adsorption capacity of fly ash preferably, showing that mercury adsorption on fly ash surface in fixed-bed is controlled dominantly by external mass transfer.

Keywords: Fly Ash, Mercury, Adsorption Equilibrium, Adsorption Kinetics, Adsorption Mechanism

INTRODUCTION

Mercury emission has attracted more and more attention because of its toxicity and bioaccumulation, which is extremely dangerous for human health [1-3]. Coal combustion is the largest source of anthropogenic mercury emissions [4,5]. In 2005, the United States Environmental Protection Agency (EPA) proposed the clean air mercury rule (CAMR) becoming the first country implementing mercury emission control [6]. Mercury, emitted from coal combustion flue gas, usually exists in three forms: elemental mercury (Hg^0), oxidized mercury (Hg^{2+}), and particle-bound mercury (Hg^P) [7,8]. 70-90% of oxidized mercury can be removed through wet flue gas desulfurization (WFGD) facilities, because oxidized mercury is highly soluble. Particulate-bound mercury can be removed with fly ash using typical particle control devices (PCDs) such as fabric filters (FFs) and electrostatic precipitators (ESPs). However, elemental mercury, which occupies around 50% of entire mercury, cannot be removed through WFGD and PCDs due to its insolubility in water and high volatility. This results in elemental mercury being nearly completely released into the atmosphere, which is harmful for human health [9]. So it is very important to remove and oxidize the elemental mercury in coal combustion flue gas.

Activated carbon injection upstream of PCDs has been recognized as a promising control technology for removing mercury from coal combustion flue gas [9-11]. However, high sorbent production cost and low sorbent utilization rate limit wide application of this technology, so developing novel sorbents with high mercury adsorption capacity and low production cost has become a hot topic [12]. Numerous studies on sorbents have been carried out, including modified activated carbon, biomass sorbent, calcium-based sorbent and fly ash etc. [5,10,12]. Among these, fly ash has been recognized as a potential mercury removal sorbent replacing activated carbon with its low cost [3,13]. Some researches on fly ash have been conducted in simulated flue gas to explore its mercury adsorption capacity and mechanism. Xu et al. [3] tested the fly ash which was modified by $CuBr_2$, $CuCl_2$ and $FeCl_3$ and found that mercury adsorption performance of fly ash was associated with its physical properties and chemical composition. Fly ash modified with $CuBr_2$, $CuCl_2$ and $FeCl_3$ is a promising sorbent for removing mercury from coal combustion flue gas. Bhardwaj [14] evaluated the impact of fly ash chemical composition on mercury adsorption in a fixed bed reactor at 140 °C and indicated that alumina, silica, calciumoxide, magnesium oxide, and titania could not promote mercury oxidation or adsorption, but ferricoxide and unburned carbon demonstrated a significant role in mercury oxidation and capture. Moreover, the research results from Hower [15], Zhao [16] and Wang [17] showed that the unburned carbon component in fly ash plays an important role in mercury adsorption capacity. Such studies provide a preliminary

†To whom correspondence should be addressed.
E-mail: yfduan@seu.edu.cn

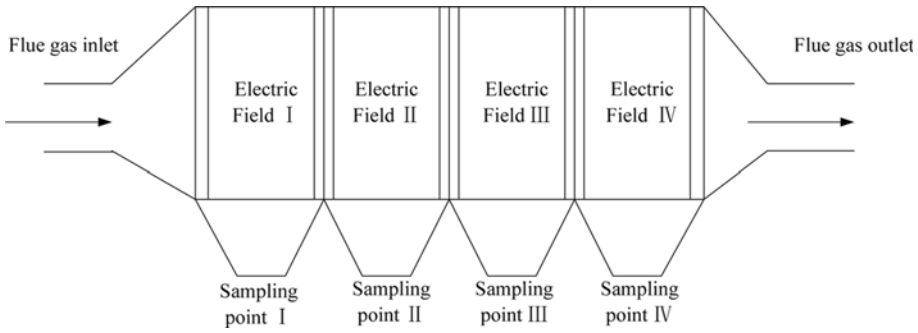

Fig. 1. Schematic of fly ash samples sampling in ESP.

understanding of mercury adsorption properties on fly ash, but there is limited literature about adsorption equilibrium and kinetics of mercury on fly ash. In addition, with highly complex nature and composition, mercury adsorption mechanism of fly ash is still not very clear and further researches are needed [18,19].

So the objective was to evaluate mercury adsorption capacity of fly ash and explore of this work mercury adsorption mechanism from adsorption equilibrium and kinetic point of view. Adsorption equilibrium and kinetic are important and effective ways to research the adsorption process, which have been widely used to study heavy metals adsorption from liquid phase and the adsorption of organic vapors, carbon dioxide, water molecules and oxygen on activated carbon [20]. In this paper samples were characterized to feature their morphologies correlated to mercury content, and experimental studies on mercury adsorption in a fixed-bed apparatus were also performed to further verify its mercury adsorption availability. Based on the experimental data, the adsorption isotherm was modeled with Langmuir, Freundlich, and Temkin equations to analyze the adsorption equilibrium properties for mercury. The Gibbs free energy change (ΔG) of the adsorption reaction was calculated to gain an insight into the mercury adsorption process. Adsorption kinetic studies were also conducted to describe the adsorption procedure and to investigate the potential adsorption rate controlling step and adsorption mechanism [20,21].

EXPERIMENTAL

1. Sample Preparation and Characterization

Four fly ash samples were collected from different siloes of the same electrostatic precipitator (ESP) of a 600 MW pulverized coal boiler firing Zhungeer bituminous coal in China shown in Fig. 1. Physical and chemical properties of the fly ash samples were characterized by various analysis techniques. The chemical composition was measured by X-ray fluorescence spectrometer (XRF). Specific surface area was obtained by adsorbing and desorbing N_2 at 77 K using an automatic volumetric multipoint apparatus (ASAP 2020, Micromeritics). The functional group species of fly ash surface were measured by Fourier transform infrared spectroscopy (FTIR). The residual carbon content was measured by heating fly ash sample to 740 °C in N_2 and then burning the sample in air for about 30 min. Mercury content was measured by Milestone DMA80 according to EPA Method 7473.

2. Mercury Adsorption Tests

The fixed-bed system, shown in Fig. 2, consisted of several com-

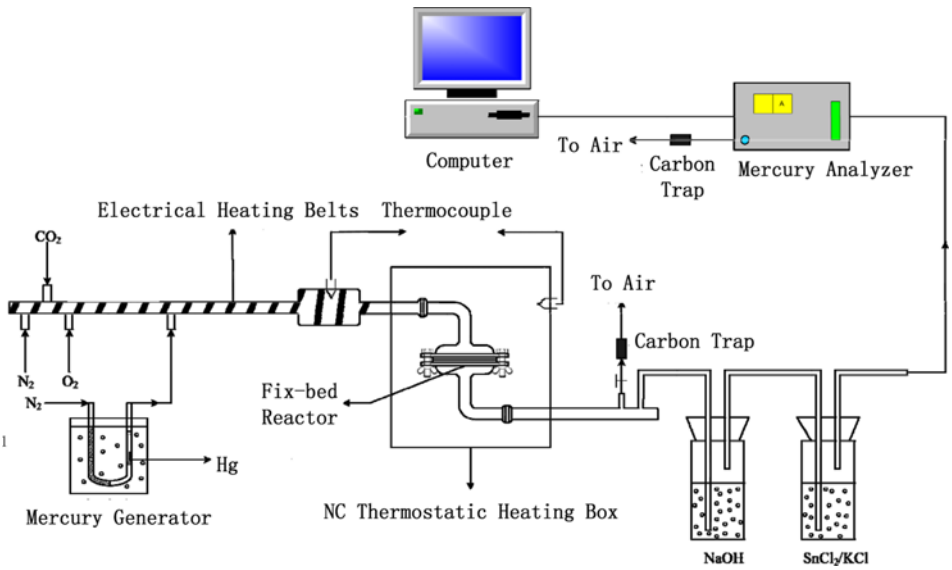

Fig. 2. Schematic of mercury adsorption fixed bed apparatus.

ponents, including Hg^0 vapor generator, fixed bed adsorption reactor, temperature control system, and Hg^0 concentration analyzer. Hg^0 is generated from a mercury permeation device (VICI Metronics Inc, USA), which is designed to produce a constant release ratio of Hg^0 vapor at the specified temperature. Nitrogen gas is supplied as carrier gas and controlled by a mass flow controller, keeping at 150 ml/min. The initial mercury concentration was adjusted at desired concentration by varying the temperature of mercury permeation device. Stability and replicate tests of inlet Hg^0 concentration confirmed that the injected Hg^0 was mixed with air flow very well and the blank Hg^0 concentration was very stable during the specified experiment time. The fixed bed adsorption reactor is constituted by quartz glass tube, enclosed in a temperature-controlled oven. The QM201H Hg^0 vapor analyzer, based on cold vapor adsorption spectrometry, is used to measure the gas phase elemental mercury concentration continuously.

The adsorption tests were conducted with 1 g fly ash packed into the quartz fixed-bed reactor. The total gas flow rate of simulated flue gas was 1.0 L/min, constituting of 6%O_2, 12%CO_2, Hg^0 vapor and nitrogen gas as equilibrium. All tests were duplicated under the same experimental condition. During each test, the initial Hg^0 concentrations (C_{in}) and the outlet Hg^0 concentrations (C_{out}) were measured. Mercury adsorption performance of fly ash samples was evaluated by constructing Hg^0 breakthrough curves and Hg^0 accumulative adsorption per unit quality. Hg^0 breakthrough rate was calculated according to equation:

$$Hg^0 \text{ penetration rate, } \% = \frac{C_{out}}{C_{in}} \times 100\% \quad (1)$$

Hg^0 accumulative adsorption per unit quality of fly ash was calculated according to equation:

$$q = \frac{Q_V}{m}\int_0^t (C_{in} - C_{out})dt \quad (2)$$

where Q_V is gas flow rate of simulated flue gas, m^3/min. m is experimental fly ash mass, g. t is adsorption reaction time, min. q is Hg^0 accumulative adsorption per unit quality of fly ash, μg/g.

RESULTS AND DISCUSSION

1. Fly Ash Characterization Results

1-1. Chemical Composition

As Table 1 shows, the fly ash sample is mainly composed of SiO_2 and Al_2O_3, as well as small amounts of other metal oxides such as Fe_2O_3 and MnO, which is the same as the results reported in the literature [22].

1-2. Physical and Chemical Properties

As Table 2 shows, fly ash particle size reduces gradually from ESP I to IV and the unburned carbon content decreases with particle size decreasing, which is consistent with the results from Lu et al. [23] and Kulatos et al. [24]. The specific surface area of fly ash increases from ESP I to IV and the mercury content first increases and then decreases. Researches [3,15,17,25] show that unburned carbon plays an important role in determining mercury adsorption capacity of fly ash. Zhao [16] and Kostova [26] indicate that unburned carbon is a core factor affecting mercury adsorption capacity, because unburned carbon in fly ash provides active sites and mercury is mainly adsorbed on the unburned carbon. Particle size is also a main factor affecting mercury adsorption [23]. Decrease of particle size reduces external mass transfer resistance of mercury adsorption on unburned carbon and increases specific surface area, which is beneficial to increase the contact change between mercury and unburned carbon. But it results in the decrease of unburned carbon content. Therefore, the mercury content increase from ESP I to IV is attributed to the reduction of mass transfer resistance, and mercury content of fly ash from ESP IV lower than that of ESP III results in low unburned carbon content.

Table 2. Physical and chemical properties of fly ash samples

Fly ash samples	Medium size $D_{0.5}$/μm	Specific surface area ($m^2 \cdot g^{-1}$)	Unburned carbon content %	Mercury content ($mg \cdot kg^{-1}$)
ESP I	140.0	1.12	1.34	0.0696
ESP II	90.0	1.36	0.92	0.2519
ESP III	12.5	1.36	0.93	0.2731
ESP IV	3.4	2	0.83	0.1967

1-3. FTIR Analysis

The Fourier transform infrared spectroscopy (FTIR) analysis of four fly ash samples was conducted. As shown in Fig. 3, the four fly ash samples have the same functional group species with seven peaks in the range of 0-4,000 cm^{-1}, including 458-461, 560-565, 744, 896-901, 1,098-1,104, 1,624 and 3,429-3,509 cm^{-1}, respectively. According to the FTIR pattern, the peak at 1,098-1,104 cm^{-1} stands for the asymmetric vibration of Al-O/Si-O, and at 744 cm^{-1} describes the bending vibration of Si-O-Si/Si-O-Al tetrahedron. In general, these chemical bonds exist in ring silicates and show similar characteristics with molecular sieve, which has adsorption ability [27]. The peak at 901 cm^{-1} illustrates the vibration absorption of Fe-containing chemical bond, and peaks at 1,623-3,429 cm^{-1} are regarded as tensile and deformation vibration of OH and H-O-H, caused by water molecules on fly ash surface [28]. Usually, peak intensity represents the content of different chemical bonds. Therefore, the content order of Al-O/Si-O, Si-O-Si/ Si-O-Al and Fe-containing chemical bonds in four fly ash samples is ESP III>ESP II>ESP IV> ESP I, which is consistent with the mercury content order listed in Table 2.

2. Mercury Adsorption Test Results

2-1. Initial Mercury Concentration Effect

As shown in Fig. 4(a), three different initial mercury concentrations were selected to estimate the effect on mercury adsorption of

Table 1. Chemical composition of fly ash sample (mass percent) /%

Sample	SiO_2	Al_2O_3	CaO	Fe_2O_3	TiO_2	K_2O	MgO	SO_3	P_2O_5	SrO	ZrO_2	MnO
Fly ash	45.1	43.3	2.85	2.41	1.56	0.58	0.28	0.23	0.21	0.17	0.15	0.03

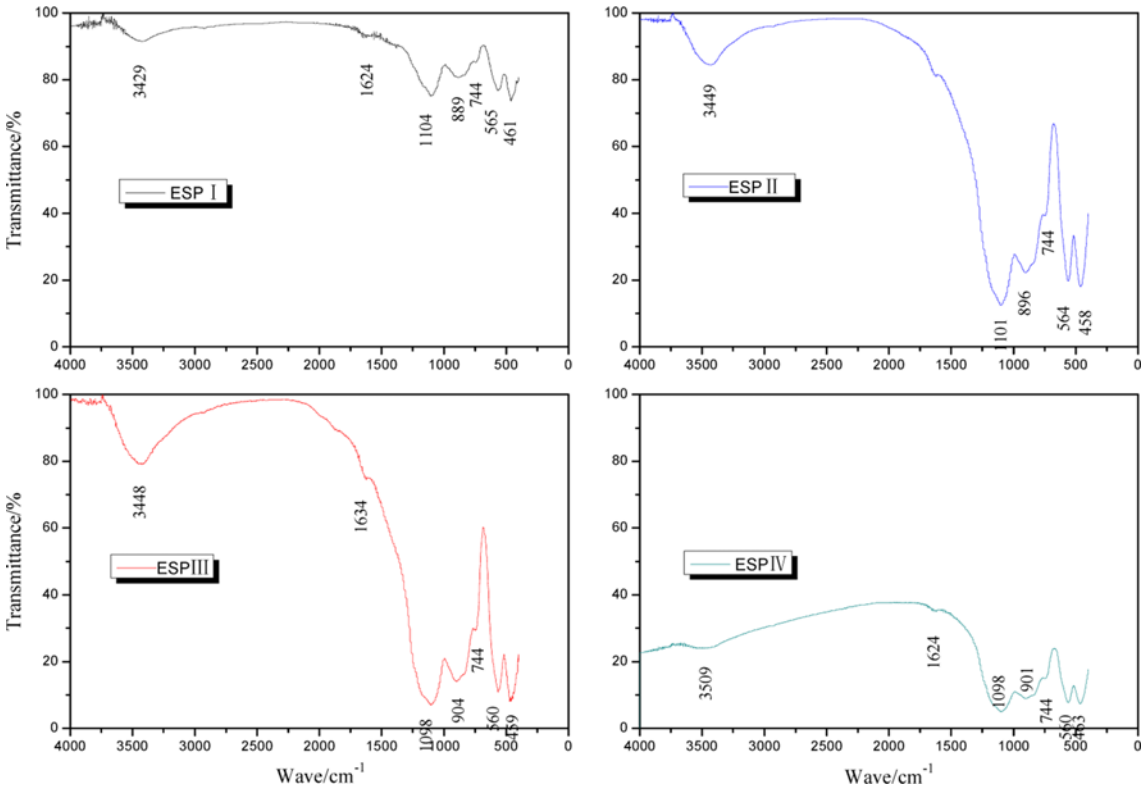

Fig. 3. FTIR spectra of four fly ash samples.

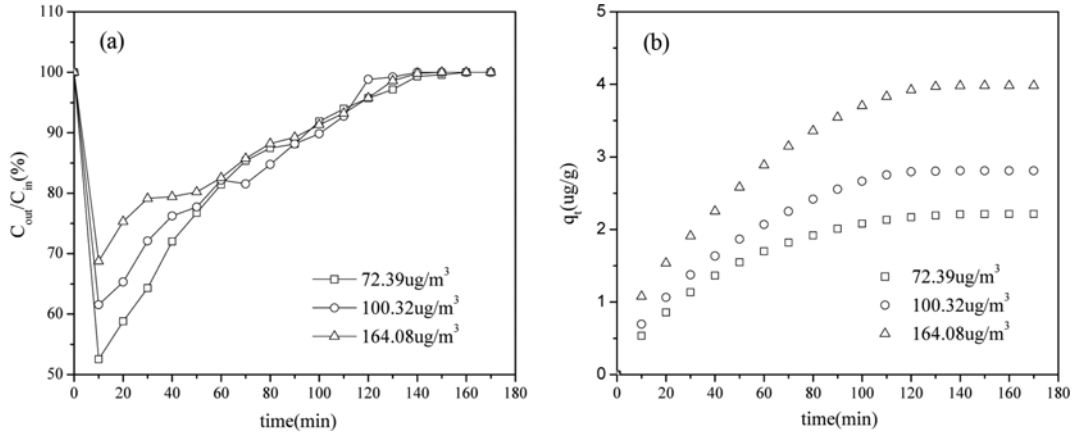

Fig. 4. Effect of initial mercury concentrations on mercury adsorption of fly ash. (a) Breakthrough curves. (b) Accumulative adsorption curves.

fly ash. The entire three mercury breakthrough curves exhibit "s" type, illustrating that mercury concentration decreases rapidly at the beginning and then slowly rises, finally recovering 100%. Fig. 4(a) also shows that increase of initial mercury concentration from 72.39 μg/m^3 to 164.08 μg/m^3 is not beneficial to promote mercury removal rate due to low mercury adsorption capacity of raw fly ash. Mercury accumulative adsorption amount is presented in Fig. 4(b), which was calculated according to Eq. (2) with 170 minutes test time. As shown in Fig. 4(b), the increase of initial mercury concentration results in the increase of mercury accumulative adsorption per unit quality of fly ash. The slope of the tangent at any point on the mercury accumulative adsorption curve stands for the mercury adsorption rate at the corresponding moment. Therefore, the "convex" type accumulative adsorption curves illustrate that fast adsorption happens in the initial stage and then mercury adsorption rate continues to reduce as the test time increases. Finally, mercury adsorption reaches saturation with adsorption rate reducing to zero.

2-2. Particle Size Effect

Mercury breakthrough curves for fly ash with different particle sizes of 25 μm-50 μm, 50 μm-74 μm, 74 μm-100 μm are given in Fig. 5(a). As shown in Fig. 5(a), all of the three mercury breakthrough curves also show "s" type. Fly ash with medium size of 50 μm-74 μm

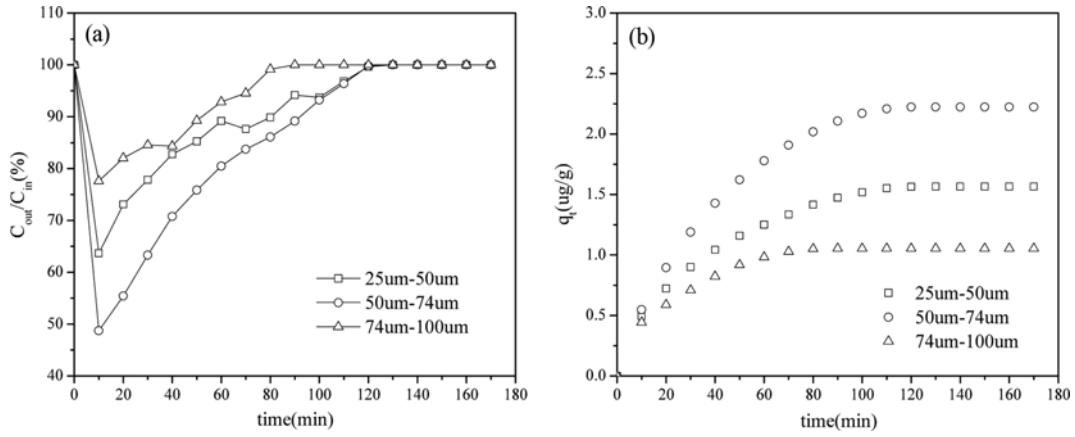

Fig. 5. Effect of particle sizes on mercury adsorption of fly ash. (a)Breakthrough curves. (b) Accumulative adsorption curves.

shows the best mercury adsorption performance, and its mercury breakthrough rate evidently is lower than the others. Fly ash with size of 74 μm-100 μm demonstrates the worst mercury adsorption performance. Mercury accumulative adsorption per unit quality of fly ash with different particle sizes is shown in Fig. 5(b). As Fig. 5(b) shows, mercury accumulative adsorption amount is low due to their small surface area and pore volume. In addition, the four fly ash samples, collected from the ESP of a power plant, contain small amount of mercury originally before mercury adsorption tests, which is another reason for resulting in low mercury adsorption capacity of raw fly ash. Fly ash with medium size of 50 μm-74 μm has the largest amount of accumulative mercury adsorption. This is because the mercury adsorption capacity of fly ash is determined mainly by unburned carbon content and particle size. Smaller particle size results in higher specific surface area, but brings about low specific surface area utilization rate for mercury adsorption due to the decrease of unburned carbon in fly ash [23,24].

3. Adsorption Equilibrium Analysis

In a fixed-bed system, a 100% mercury breakthrough rate illustrates that the outlet mercury concentrations (C_{out}) equal the inlet mercury concentrations (C_{in}) with mercury reaching adsorption saturation on fly ash. At adsorption equilibrium, the inlet mercury concentration can be considered as the equilibrium concentration, and the saturated mercury adsorption capacity of fly ash can be considered as the equilibrium adsorption capacity.

Three widely used adsorption isotherm equations, Langmuir, Freundlich, and Temkin, were utilized for fitting the experimental data. The deviation between experimental and calculated data is expressed by the correlation coefficient R^2. Since experimental data is forced to fit the equation, a greater R^2 value indicates an isotherm equation describing the adsorption process more closely [20].

The Langmuir isotherm equation is used to describe physisorption and chemisorption. It is based on the assumption that interaction forces between the adsorbed molecules are negligible and the sorbent surface is homogeneous with identical adsorption sites:

$$q_e = \frac{q_m K_A C_e}{1 + K_A C_e} \tag{3}$$

where q_m is the maximum adsorption capacity, μg/g. q_e is adsorption capacity at equilibrium, μg/g. K_A is a constant related to adsorption free energy, L/mmol. C_e is equilibrium mercury concentration, mmol/L. A simplified equation is shown as follows:

$$\frac{1}{q_e} = \frac{1}{q_m} + \frac{1}{q_m K_A}\frac{1}{C_e} \tag{4}$$

The Freundlich isotherm equation is also suitable for describing physisorption and chemisorption. It is an empirical equation considering heterogeneous adsorption on the sorbent surface:

$$q_e = K_F C_e^{1/n} \tag{5}$$

where K_F and n are Freundlich parameters dependent on temperature and adsorption intensity, respectively. The 1/n value determines the degree of adsorption. Fox example, the 1/n value is in the range of 0.1-0.5, illustrating ease of adsorption, and the 1/n value is more than 2, indicating difficulty of adsorption. A linear equation is shown as follows:

$$\ln q_e = \ln K_F + \frac{1}{n}\ln C_e \tag{6}$$

The Temkin isotherm equation can only be used to describe chemisorption. The equation assumes that adsorption heat reduces linearly with adsorption capacity increases due to the interaction of adsorbate and sorbent. Moreover, the adsorption binding energy is distributed evenly:

$$q_e = \frac{RT}{\beta}\ln(K_T C_e) \tag{7}$$

A linear equation is obtained by taking the logarithm on the right hand of of Eq. (7)

$$q_e = B_1 \ln K_T + B_1 \ln C_e \tag{8}$$

$$B_1 = \frac{RT}{\beta} \tag{9}$$

where K_T is an equilibrium parameter corresponding to the maximum binding energy, L/g; B_1 is a dimensionless constant related to temperature and adsorption system.

The fitting curves of the three equations are shown in Fig. 6 and Fig. 7 with the parameters and correlation coefficient R^2 summa-

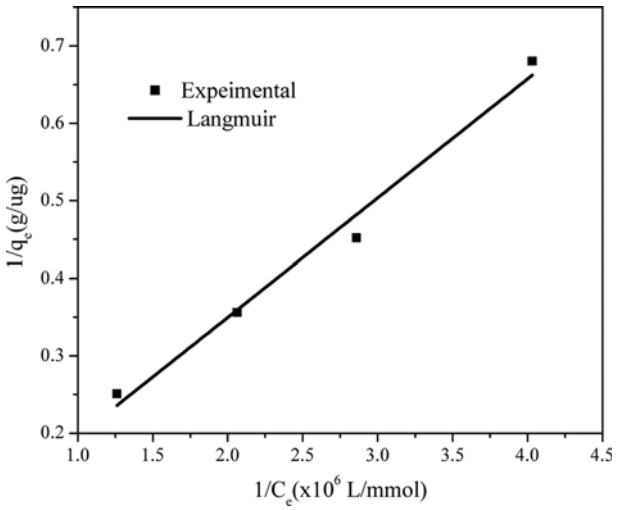

Fig. 6. Fitting of Langmuir isotherm equation.

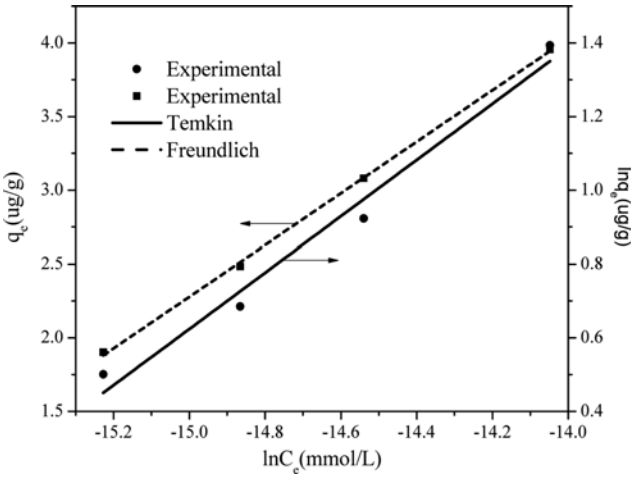

Fig. 7. Fitting of Freundlich and Temkin isotherm equations.

rized in Table 3. Of these models, the Freundlich equation gives the best fitting performance, illustrating that it can predict mercury adsorption equilibrium on fly ash more accurately, indicating non-uniform properties of the fly ash surface. The parameter of 1/n in the Freundlich equation is equal to 0.69, illustrating that mercury can be adsorbed by fly ash easily. The Langmuir and Temkin equations can also predict the mercury adsorption equilibrium on fly ash surface well, but worse than the Freundlich equation.

The Gibbs free energy change (ΔG) of adsorption reaction is calculated by the following thermodynamic equation:

$$\Delta G = -RT \ln K_A \quad (10)$$

where R is gas constant (8.314J/(mol·K)), T is reaction temperature in Kelvin (K) and K_A (L/mmol) is from Langmuir equation [21]. Obviously, the ΔG value obtained in Eq. (10) is negative, revealing the spontaneous nature of the adsorption reaction. Generally, the ΔG value is in the range of 0 to −20 kJ/mol, indicating physical adsorption and −80 to −400 kJ/mol representing chemical adsorption [21]. In this study, the ΔG value is −36.73 kJ/mol, indicating that mercury adsorption of fly ash at 120 °C is mainly physical enhanced by chemisorption.

4. Adsorption Kinetic Analysis

Kinetic analysis can reveal the adsorption mechanism and predict the adsorption rate controlling step. Three basic steps are involved in mercury adsorption on fly ash: transport of mercury from bulk-gas phase to external surface of fly ash (external mass transfer), intraparticle diffusion of mercury to activate sites (intraparticle diffusion), and mercury adsorption at activate sites [29]. The adsorption rate controlling step is dependent on the slowest rate.

Three simplified kinetic models were used to fit the experimental data. The effects of initial mercury concentration and fly ash particle size on mercury adsorption were analyzed from the kinetic point of view. The deviation between experimental and calculated data was expressed by the correlation coefficient R^2. Since the experimental data were forced to fit the equation, a greater R^2 value indicated that the adsorption kinetic model can describe the adsorption process more closely [20].

4-1. Weber and Morris Intraparticle Diffusion Model

The Weber and Morris model, derived from a mass balance equation, is usually used to describe intraparticle diffusion process and solve the internal diffusion coefficient. It is expressed as follows [30]:

$$q_t = k_{id} t^{1/2} + C \quad (11)$$

where q_t is mercury uptake at time t, μg/g. k_{id} is intraparticle diffusion coefficient, μg/(g·min$^{1/2}$), C is a constant related to the thickness of boundary layer, μg/g. t is reaction time, min.

Table 3. Parameters from linear fitting by Langmuir, Freundlich and Temkin isotherm equations

Langmuir			Freundlich			Temkin		
q_m (μg/g)	K_A (L/mmol)	R^2	K_F (μg·L$^{1/n}$(g·mmol$^{1/n}$)$^{-1}$)	n	R^2	B_1	K_T (μg·L(mmol·g)$^{-1}$)	R^2
23.87	0.2722×10^6	0.9782	7.313×10^4	1.449	0.9991	1.908	9.622×10^6	0.9705

Table 4. Kinetic parameters obtained from intraparticle diffusion model

Initial mercury concentration (μg/m^3)	k_{id} (μg/(g·min$^{1/2}$))	C (μg/g)	R^2	Size (μm)	k_{id} (μg/(g·min$^{1/2}$))	C (μg/g)	R^2
72.39	0.1800	0.1496	0.9472	25-50	0.1209	0.2041	0.9263
100.32	0.2324	0.1367	0.9545	50-74	0.1801	0.1965	0.9234
164.08	0.3266	0.1931	0.9646	74-100	0.0733	0.2647	0.8174

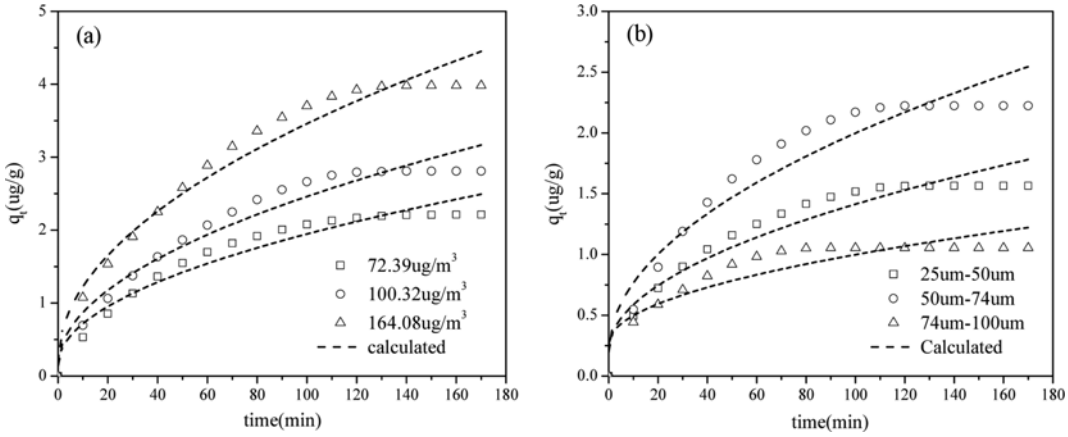

Fig. 8. Fitting of intraparticle diffusion equation. (a) Initial mercury concentration. (b) Particle size.

The fitting results are given in Fig. 8 and the calculated kinetic parameters are presented in Table 4. Fig. 8 shows that the deviations between fitting curves and experimental data are large, which is confirmed by the low correlation coefficient R^2 value presented in Table 4. As Table 4 shows, the R^2 value of all conditions is lower than 0.964, which indicates that the intraparticle diffusion kinetic model cannot describe the process of mercury adsorption on fly ash very well. Table 4 also shows that the mercury intraparticle diffusion coefficient k_{id} is reduced continuously as the initial mercury concentration decreases. Fly ash with medium particle size of 50 μm-74 μm has greater intraparticle diffusion coefficient k_{id} compared to the fly ash samples with particle size of 25-50 μm and 74-100 μm.

4-2. Pseudo-first-order Kinetic Model

A pseudo-first-order kinetic model, also derived from mass balance equation, is usually used to describe external mass transfer process and predict equilibrium adsorption capacity [20,31]:

$$\frac{dq_t}{d} = k_1(q_e - q_t) \tag{12}$$

According to the boundary conditions of t=0, q_t=0 and t=t, q_t= q_t, a simplified equation is obtained by integrating Eq. (12)

$$q_t = q_e(1 - e^{-k_1 t}) \tag{13}$$

where q_t and q_e are mercury uptake at time t and at equilibrium, respectively, μg/g; and k_1 is the rate constant of pseudo-first-order equation, min^{-1}; t is reaction time, min.

The fitting results are given in Fig. 9 and calculated parameters are presented in Table 5. As shown in Fig. 9, a good agreement between calculated and experimental mercury uptake curves is achieved, which is verified by the high correlation coefficient R^2 value pre-

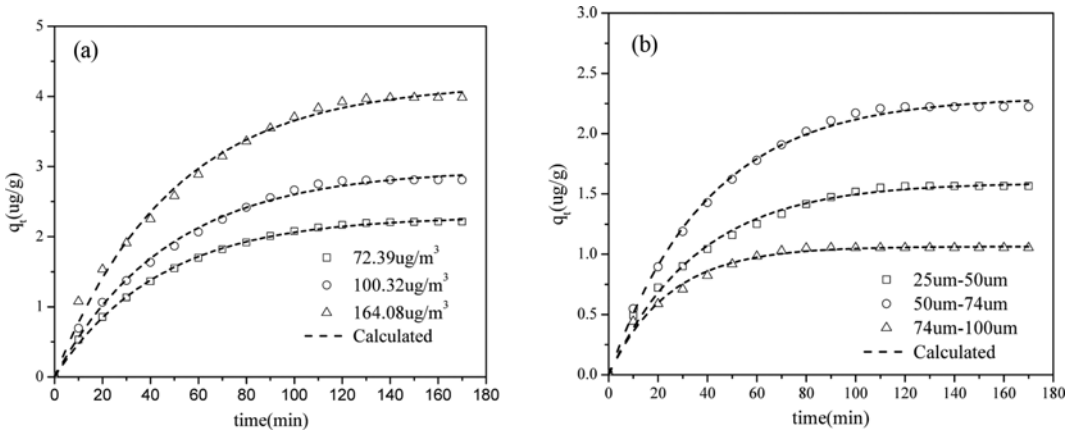

Fig. 9. Fitting of pseudo-first-order equation. (a) Initial mercury concentration. (b) Particle size.

Table 5. Kinetic parameters obtained from pseudo-first-order model

Initial mercury concentration (μg/m^3)	q_e (μg/g)	k_1 (min^{-1})	R^2	Size (μm)	q_e (μg/g)	k_1 (min^{-1})	R^2
72.39	2.288	0.0231	0.9988	25-50	1.594	0.0279	0.9934
100.32	2.960	0.0211	0.9951	50-74	2.306	0.0250	0.9975
164.08	4.190	0.0206	0.9926	74-100	1.064	0.0412	0.9906

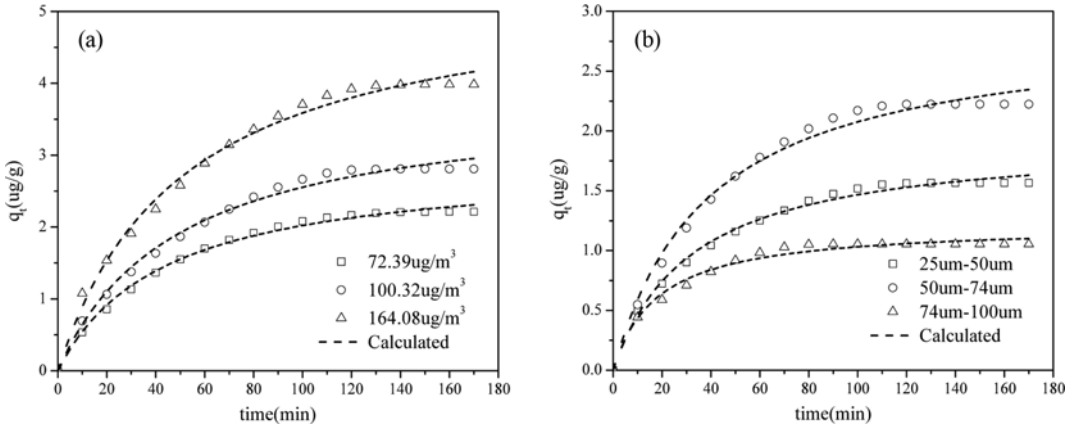

Fig. 10. Fitting of pseudo-second-order equation. (a) Initial mercury concentration. (b) Particle size.

Table 6. Kinetic parameter obtained from pseudo-second-order model

Initial mercury concentration (μg/m^3)	q_e (μg/g)	$k_2q_e^2$ (μg/(g·min))	R^2	Size (μm)	q_e (μg/g)	$k_2q_e^2$ (μg/(g·min))	R^2
72.39	2.898	0.0663	0.9948	25-50	1.938	0.0605	0.9932
100.32	3.807	0.0768	0.9911	50-74	2.882	0.0739	0.9888
164.08	5.398	0.1049	0.9917	74-100	1.217	0.0231	0.9827

sented in Table 5: the R^2 value of all conditions is higher than 0.9906, which indicates that the pseudo-first-order kinetic model can describe the process of mercury adsorption on fly ash very well and external mass transfer is the adsorption rate controlling step compared to intraparticle diffusion process.

Table 5 also shows that the calculated equilibrium uptake q_e continues to increase with initial mercury concentration increase, and fly ash with medium particle size of 50 μm-74 μm has the greatest equilibrium uptake q_e, which is consistent with experimental results. In addition, increase of initial mercury concentration results in the correlation coefficient R^2 decreasing, which indicates that the controlling role of external mass transfer is in weakening as initial mercury concentration increases. In other words, increase of initial mercury concentration reduces external mass transfer resistance.

4-3. Pseudo-second-order Kinetic Model

The pseudo-second-order kinetic model, based on the Langmuir adsorption isotherm equation, focuses on describing chemisorption at activated sites. In this model, chemisorption is the adsorption rate controlling step. The pseudo-second-order kinetic model can be expressed as follows: [20,32]

$$\frac{dq_t}{dt} = k_2(q_e - q_t)^2 \quad (14)$$

According to the boundary conditions of t=0, q_t=0 and t=t, q_t= q_t, a simplified equation is obtained by integrating Eq. (14).

$$q_t = \frac{t}{1/(k_2q_e^2) + t/q_e} \quad (15)$$

where q_t and q_e are mercury uptake at time t and at equilibrium, respectively, μg/g. k_2 is the adsorption rate constant of pseudo-second-order equation, g/(μg·min); t is reaction time, min. $k_2q_e^2$ is considered to be initial adsorption rate, μg/(g·min).

The fitting results are given in Fig. 10 and calculated parameters are presented in Table 6. As shown in Table 6, the increase of initial mercury concentration is beneficial to promote the equilibrium adsorption uptake q_e and the initial adsorption rate $k_2q_e^2$ increasing. Fly ash with medium size of 50-74 μm has the greatest q_e and $k_2q_e^2$, but fly ash with size of 74-100 μm has the worst results. Fig. 10 shows that the pseudo-second-order kinetic model can fit experimental data well, which is confirmed by the high correlation coefficient R^2 presented in Table 6. It illustrates that the pseudo-second-order kinetic model can also describe the process of mercury adsorption on fly ash well. However, the correlation coefficient R^2 presented in Table 6 is lower slightly than that presented in Table 5 and calculated mercury uptake q_e of pseudo-first-order model is closer to experimental data. Therefore, it can be concluded that external mass transfer is adsorption rate controlling step and chemisorption also plays an important role in mercury adsorption on fly ash. Since pseudo-second order kinetic model is from Langmuir adsorption isotherm equation, high correlation coefficient R^2 demonstrates that mercury adsorption on fly ash follows the Langmuir isotherm equation.

CONCLUSIONS

Fly ash samples were collected from the electrostatic precipitator (ESP) of a 600 MW pulverized coal boiler firing Zhungeer bituminous coal in China to evaluate and explore its mercury adsorption ability. Fly ash samples characterization, fixed-bed mercury adsorption tests, adsorption equilibrium and kinetics studies were conducted to investigate mercury adsorption mechanism. The obtained results are listed as follows:

1) Mercury content of fly ash samples is associated with particle size and unburned carbon content. The functional groups of

Al-O/Si-O or Si-O-Si/Si-O-Al tetrahedron on fly ash surface also play some role in mercury adsorption.

2) Increase of initial mercury concentration is beneficial to promote mercury adsorption capacity of fly ash, due to the enhancement of mercury diffusion force onto the fly ash surface, mercury intraparticle diffusion rate and initial mercury adsorption rate. The sorbent with higher mercury adsorption capacity usual has higher initial mercury adsorption rate.

3) Fly ash with medium size shows the best mercury adsorption capacity. Smaller particle size results in higher specific surface area, but brings about low specific surface area utilization rate for mercury adsorption due to the decrease of unburned carbon.

4) The Freundlich isotherm equation presents the best fitting result in three isotherm equations, indicating the non-uniformity properties of fly ash surface. Mercury adsorption on fly ash at 120 °C is mainly physisorption but enhanced by chemisorption.

5) The pseudo-first-order adsorption kinetic model can describe the adsorption process more accurately and predict mercury adsorption capacity of fly ash better, showing that mercury adsorption on fly ash is controlled predominantly by external mass transfer, and chemisorption also plays an important role in mercury adsorption.

ACKNOWLEDGEMENTS

This study was supported by National Nature Science Foundation of China (51376046, 51076030), the Fundamental Research Funds for the Central Universities; Graduate Student Research and Innovation Program of Jiangsu Province (KYLX_0115, CXZZ13_0093, KYLX_0184), National Science and Technology Support Program of China (2012BAA02B01-02), Jiangsu Province United Creative Subject (BY2013073-10).

REFERENCES

1. S. Bose-O'Reilly, B. Lettmeier, R. M. Gothe, C. Beinhoff, U. Siebert and G. Drasch, *Environ. Res.*, **107**, 89 (2008).
2. H. C. Hsi, C. Y. Tsai, T. H. Kuo and C. S. Chiang, *Bioresour. Technol.*, **102**, 7470 (2011).
3. W. Q. Xu, H. R. Wang and T. Y. Zhu, *J. Environ. Sci.*, **25**, 393 (2013).
4. A. B. Mukherjee, R. Zevenhoven, P. Bhattacharya, K. S. Sajwand and R. Kikuchie, *Resour., Conserv. Recycl.*, **52**, 571 (2008).
5. J. L. Ren, J. S. Zhou, Z. Y. Luo, C. X. Hu and Y. J. Zhong, *Proceedings of the Chinese Society of Electrical Engineering*, **27**, 48 (2007).
6. Y. Zhuang, J. S. Thompson, C. J. Zygarlicke and J. H. Pavlish, *Fuel*, **86**, 2351 (2007).
7. A. I. Martinez and B. K. Deshpande, *Fuel Process. Technol.*, **88**, 982 (2007).
8. Y. J. Wang, Y. F. Duan, L. G. Yang, Y. M. Jiang, C. J. Wu, Q. Wang and X. H. Yang, *J. Fuel Chem. Technol.*, **36**, 23 (2008).
9. S. H. Lee, Y. J. Rhim, S. P. Cho and J. I. Baek, *Fuel*, **85**, 219 (2006).
10. S. B. Ghorishi, R. M. Keeney, S. D. Serre, B. K. Gullett and W. S. Jozewicz, *Environ. Sci. Technol.*, **36**, 4454 (2002).
11. Y. Zheng, A. D. Jensen, C. Windelin and F. Jensen, *Prog. Energy Combust. Sci.*, **38**, 599 (2012).
12. H. Yang, Z. Xu, M. Fan and R. R. Judkins, *J. Hazard. Mater.*, **146**, 1 (2007).
13. A. A. Presto and E. J. Granite, *Environ. Sci. Technol.*, **40**, 5601 (2006).
14. R. Bhardwaj, X. Chen and R. D. Vidic, *J. Air Waste Manage. Assoc.*, **59**, 1331 (2009).
15. J. C. Hower, C. L. Senior, E. M. Suuberg, R. H. Hurt, J. L. Wilcoxd and E. S. Olsone, *Prog. Energy Combust. Sci.*, **36**, 510 (2010).
16. Y. C. Zhao, J. Y. Zhang, J. Liu, M. Diaz-Somoano, P. Abad-Valle, M. R. Martinez-Tarazona and C. G. Zheng, *Science China Technological Sciences,* **53**, 976 (2010).
17. S. Wang and H. Wu, *J. Hazard. Mater.*, **136**, 482 (2006).
18. M. Li, J. Liu and C. G. Zheng, *J. Eng. Thermophys.*, **28**, 882 (2007).
19. M. A. Lopez-Anton, P. Abad-Valle, M. Diaz-Somoano, I. Suarez-Ruiz and M. R. Martinez-Tarazona, *Fuel*, **88**, 1194 (2009).
20. G. Skodras, I. Diamantopoulou, G. Pantoleontos and G. P. Sakellaropoulos, *J. Hazard. Mater.*, **158**, 1 (2008).
21. Q. S. Liu, T. Zheng, P. Wang, J. P. Jiang and N. Li, *Chem. Eng. J.*, **157**, 348 (2010).
22. F. Goodarzi, *Fuel*, **85**, 1418 (2006).
23. Y. Q. Lu, M. Rostam-Abadi, R. Chang, C. Richardson and J. Paradis, *Energy Fuels*, **21**, 2112 (2007).
24. I. Kulatos, R. H. Hurt and E. M. Subberg, *Fuel*, **83**, 223 (2004).
25. S. Li, C. M. Cheng, B. Chen, Y. Cao, J. Vervcynckt, A. Adebambo and W. P. Pan, *Energy Fuels*, **21**, 3292 (2007).
26. I. Kostova, C. Vassileva, S. F. Dai, J. C. Hower and D. Apostolova, *Int. J. Coal Geology*, **116-117**, 227 (2013).
27. J. C. Swanepoel and C. A. Strydom, *Appl. Geochem.*, **17**, 1143 (2002).
28. A. Palomo, M. T. Blanco-Varela, M. L. Granizo, F. Puertas, T. Vazquez and M. W. Grutzeck, *Cem. Concr. Res.*, **29**, 997 (1999).
29. S. D. Serre, B. K. Gullett and S. B. Ghorishi, *J. Air Waste Manage. Assoc.*, **51**, 733 (2001).
30. Y. Yin, J. Zhang and C. Sheng, *Zhongguo Proceedings of the Chinese Society of Electrical Engineering*, **30**, 49 (2010).
31. A. S. Ozcan and A. Ozcan, *J. Colloid Interface Sci.*, **276**, 39 (2004).
32. S. Wang and H. Li, *J. Hazard. Mater.*, **126**, 71 (2005).